

Electron-paramagnetic-resonance identification of the manganese-gallium pair in silicon

J. Kreissl, K. Irmischer, and W. Gehlhoff

Academy of Sciences, Center for Scientific Instruments, Rudower Chaussee 6, Berlin 1199, Federal Republic of Germany

P. Omling and P. Emanuelsson

Department of Solid State Physics, University of Lund, Box 118, S-221 00 Lund, Sweden

(Received 30 January 1991)

An electron-paramagnetic-resonance (EPR) investigation of silicon doped with gallium and manganese shows a defect-related spectrum with trigonal symmetry. The proof that Mn and Ga are involved in the defect is based on the observed hyperfine interactions. A complicated fine-structure behavior results from the fact that the zero-field and Zeeman splittings are of similar magnitude, a so-called intermediate case. The analysis of the experimental data gives strong evidence that the defect is a nearest-neighbor pair of interstitial Mn and substitutional Ga, and that the EPR spectrum originates from the ${}^6S_{5/2}$ ground state of the Mn^{2+} ion in a crystal field of tetrahedral symmetry with a strong trigonal distortion, i.e., from a $(Mn_i^{2+}Ga_s^-)$ pair. A comparison between different Mn-acceptor pairs suggests that the size of the pairing acceptor is the main reason for the observed differences in the strength of the trigonal zero-field splitting.

INTRODUCTION

Electron-paramagnetic-resonance (EPR) investigations of manganese and manganese-related defects in silicon have contributed substantially to the understanding of the properties of transition metals in silicon. From EPR investigations manganese is known to appear as isolated point defects in different charge states in both interstitial and substitutional lattice sites, in pairs with acceptors as well as in clusters.¹⁻⁵ The results obtained from these investigations, space-charge measurements,⁶⁻⁸ optical measurements,^{9,10} and from theoretical studies^{11,12} have given a comprehensive picture of the electronic structure of Mn-related defects.

The successful studies of pairs of iron and group-III acceptors have resulted in a renewed interest in EPR investigations of the corresponding Mn-acceptor pairs.^{3,13-16} For instance, the question whether or not the Mn-acceptor pairs show metastable properties similar to the Fe-acceptor pairs^{14,17,18} is of considerable interest. Mn-B and Mn-Al pairs are already known from the pioneering work by Ludwig and Woodbury,¹ but only the Mn-B pair has been investigated in detail.² Recently, also, the Mn-In pair was thoroughly studied in an EPR investigation.³ In contrast to the Fe-group-III acceptor pairs, the Mn-group-III acceptor pairs apparently show no metastability. The EPR spectra obtained on the positively charged Mn-acceptor pairs show trigonal symmetry and are interpreted as being due to a nearest-neighbor pair of Mn_i^{2+} and B_S^- , Al_S^- , or In_S^- , respectively. The spectra are successfully analyzed using a spin Hamiltonian with $S = \frac{5}{2}$, corresponding to a model in which the spin properties originate from the ${}^6S_{5/2}$ ground state of a Mn^{2+} ion in a trigonally distorted cubic crystal field.

The electrical behavior of the Mn-B pair has been characterized by space-charge techniques⁶ and a combination of space-charge and EPR investigations.¹⁹ The

position of the $(Mn-B)^{+/0}$ energy level has been determined to be $E_c - 0.5$ eV. Similar midgap positions have been reported for the corresponding Mn-Al and Mn-Ga levels.²⁰

In contrast to the other Mn-acceptor pairs, EPR data on the Mn-Ga pair have not been reported. We have, therefore, searched for such a defect by codoping Si samples with Mn and Ga. An EPR spectrum showing great complexity has thus been discovered. In this paper the spectrum will be identified as a trigonal pair of Mn and Ga, and the analysis will show that the spectrum arises from the ground-state manifold of the $(Mn^{2+}-Ga^-)$ defect. Finally, the trigonal zero-field-splitting parameters obtained for the $(Mn-Ga)^+$ pair will be compared with the corresponding parameters of the other Mn-acceptor pairs.

EXPERIMENT

The samples were prepared from Czochralski-grown, gallium-doped silicon crystals with a Ga content of 10^{17} – 10^{18} cm⁻³. The manganese doping was performed by encapsulating metallic manganese and a carefully etched {110}-oriented Si:Ga sample in an evacuated quartz ampule. The manganese was allowed to diffuse for 1 h at 1150 °C, and the sample was thereafter rapidly quenched by dropping the ampule into water.

The EPR measurements were performed in the X band using a ZWG ERS 230 spectrometer equipped with fixed-temperature cryostats ($T=20.4$ and 1.4 K) and a Bruker ESP 300 spectrometer equipped with a He-gas-flow cryostat for measurements at different temperatures.

EXPERIMENTAL RESULTS AND ANALYSIS

A complicated EPR spectrum was observed in samples codoped with Mn and Ga. The spectrum, which depends

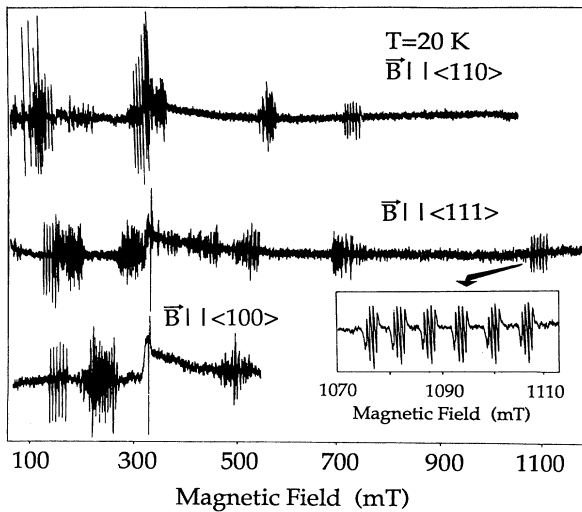


FIG. 1. Experimental EPR spectra of the $(\text{Mn}^{2+}\text{-Ga}^-)$ pair for the three main directions, obtained at $T=20$ K and using a microwave frequency of 9.239 GHz. The single resonance at 329 mT is due to the surface signal.

strongly on the angle between the crystal axes and the magnetic field, is shown for the three main directions ($\vec{B} \parallel \langle 110 \rangle$, $\langle 111 \rangle$, and $\langle 100 \rangle$) in Fig. 1. The sixfold hyperfine splitting observed for some transitions in the main directions proves the involvement of one Mn atom ($I = \frac{5}{2}$, 100% natural abundance) in the defect. The high-field, fine-structure transition for $\vec{B} \parallel \langle 111 \rangle$ ($\theta = 0^\circ$; θ is the angle between the magnetic field and the trigonal C_3 axis) shown in the inset in Fig. 1 reveals a further splitting of each Mn hyperfine line into mainly four components. This shows that a second atom with nuclear spin $I = \frac{3}{2}$ is part of the defect, and as will be described below, a detailed analysis of this hyperfine interaction, including the effects of the natural isotope content of Ga, unambiguously proves that one Ga is part of the defect. This reasoning is based on the fact that only the allowed nuclear spin transitions of manganese and gallium ($\Delta m_{\text{Mn, Ga}} = 0$) are of importance in this particular direction.

For arbitrary directions the manganese and gallium hyperfine interactions become very complicated because of the simultaneous occurrence of allowed and forbidden hyperfine transitions. This is due to a strong mixing of the nuclear states. The reasons for this mixing are the same as those reported in the cases of Mn-B and Mn-In.^{2,3}

The measured angular dependences of the electronic spin transitions are plotted as solid circles on the right in Fig. 2. The solid circles represent the fine-structure positions, which have been estimated as the center of gravity of the observed hyperfine-structure transitions. Also, the intensity of the transitions depends strongly on the angle

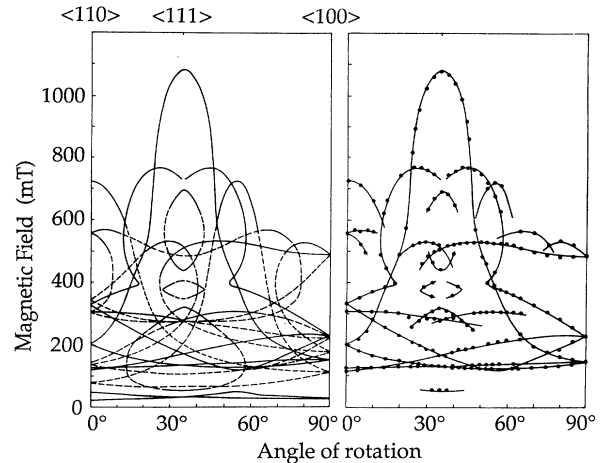


FIG. 2. Angular dependence of fine-structure line positions of the $(\text{Mn}^{2+}\text{-Ga}^-)$ pair obtained at 9.01 GHz. The magnetic field is rotated in the $\{110\}$ crystal plane. Left side, plot of all possible fine-structure transitions. The dashed lines reflect transitions with a low transition probability. Right side, the experimental data are indicated by solid circles. In order to facilitate a comparison with the left figure, the parts of the calculated angular dependence for which experimental data exist are indicated by thin solid lines. It should be noted that also the calculated intensities agree with the experimental ones.

between the magnetic field and crystal axes. Therefore, in many cases the lines cannot be observed for all directions. On the other hand, these intensity variations are of great importance when assigning the fine-structure lines to specific spin transitions.

For $(\text{Mn-Al})^+$, $(\text{Mn-B})^+$, and $(\text{Mn-In})^+$, the analyses of the fine-structure spectra were simplified by the fact that they represent two extreme cases.¹⁻³ The $(\text{Mn-B})^+$ and $(\text{Mn-Al})^+$ are examples for which the weak crystal-field approximation is valid, while $(\text{Mn-In})^+$ shows a behavior, at least for the transitions within the $S = \frac{1}{2}$ doublet, typical of the strong crystal-field approximation. In the case of $(\text{Mn-Ga})^+$, the spectrum is much more complicated and gives no simple picture of the behavior of an expected trigonally distorted $\text{Mn}^{2+}(3d^5)$ ion in any of these limiting cases. As will be shown in the analysis below, the spectrum is, instead, a clear example of an intermediate case, where the Zeeman and the zero-field splittings are of comparable magnitude.

On the assumption that the $(\text{Mn-Ga})^+$ pair shows the same defect structure as the other Mn-acceptor pairs, the EPR spectrum will be caused by electronic spin transitions within the ${}^6S_{5/2}$ ground state of a $3d^5$ manganese ion which experiences a trigonal distortion of its tetrahedral symmetry from an associated gallium ion. The spin Hamiltonian of such a manganese-gallium pair can be written as²¹

$$H = H_Z + H_{\text{CF}} + H_{\text{Mn}} + H_{\text{Ga}}, \quad (1)$$

$$H_Z = g_{\parallel} \mu_B B_z S_z + g_{\perp} \mu_B (B_x S_x + B_y S_y), \quad (2)$$

$$H_{CF} = D[S_z^2 - \frac{1}{3}S(S+1)] - [(a-F)/180]\{35S_z^4 - [30S(S+1) - 25]S_z^2 - 6S(S+1) + 3S^2(S+1)^2\} \\ + (a2^{1/2})/36[S_z(S_+^3 + S_-^3) + (S_+^3 + S_-^3)S_z], \quad (3)$$

$$H_{Mn} = A_{Mn}S_zI_z^{Mn} + B_{Mn}(S_xI_x^{Mn} + S_yI_y^{Mn}), \quad (4)$$

$$H_{Ga} = A_{Ga}S_zI_z^{Ga} + B_{Ga}(S_xI_x^{Ga} + S_yI_y^{Ga}), \quad (5)$$

where all symbols have their usual meanings. Here the nuclear quadrupole and nuclear Zeeman interactions have been neglected. The z axis of the coordinate system (x, y, z) coincides with the pair axis aligned with the C_3 crystalline direction, and the x and y axes are chosen according to Ref. 22; e.g., for $z \parallel [111]$, the x and y axes are given by $x \parallel [\bar{1}\bar{1}2]$ and $y \parallel [1\bar{1}0]$. According to the four C_3 directions there are four different center positions, two of which are always magnetically equivalent for rotation around the $\langle 110 \rangle$ axis (as was done in our experiments). Since perturbation theory cannot be used for arbitrary directions in a truly intermediate case, we have applied the method of direct diagonalization of the $S = \frac{5}{2}$ energy matrix. Using a computer procedure for the calculation of eigenvalues and eigenfunctions for a spin Hamiltonian, including the electronic Zeeman and the zero-field interaction terms [Eqs. (2) and (3)], good agreement between the measured and calculated line positions and intensities could be obtained for the whole angular dependence of the fine-structure transitions. The results of the theoretical calculations are shown in Fig. 2. On the left all possible EPR transitions are included as solid lines for large transition probabilities and as dashed lines for transitions with smaller transition probabilities. On the right in Fig. 2, the calculated curves for which experimental data exist are drawn as solid lines in order to show the good agreement between theory and experiment. This good agreement also excludes the possibility that there are other Mn-related lines in the spectrum. The parameters g_{\parallel} , g_{\perp} , D , and $a-F$, which were found to give the best fit of the experimental points, are given in Table I.

It should be noted that the electronic spin quantum numbers M defined by the trigonal crystal-field axis are not good quantum numbers in the range of the magnetic field in which the spin transitions occur. In order to keep track of the energy levels in the discussion, we will designate them by the high-magnetic-field quantum numbers.

TABLE I. Spin Hamiltonian parameters of $Mn_i^{2+}-Ga_s^{-}$.

| | |
|---------------------------------|--|
| g_{\parallel} | 2.004 ± 0.005 |
| g_{\perp} | 2.004 ± 0.005 |
| D | $0.1773 \pm 0.0005 \text{ cm}^{-1}$ |
| $D(Mn-^{71}Ga) - D(Mn-^{69}Ga)$ | $-(0.06 \pm 0.005) \times 10^{-4} \text{ cm}^{-1}$ |
| $a-F$ | $0.0025 \pm 0.0005 \text{ cm}^{-1}$ |
| $ A_{Mn} $ | $(53.2 \pm 0.5) \times 10^{-4} \text{ cm}^{-1}$ |
| $ B_{Mn} $ | $(53.2 \pm 0.5) \times 10^{-4} \text{ cm}^{-1}$ |
| $ A_{^{69}Ga} $ | $(5.83 \pm 0.03) \times 10^{-4} \text{ cm}^{-1}$ |
| $ A_{^{71}Ga} $ | $(7.40 \pm 0.03) \times 10^{-4} \text{ cm}^{-1}$ |
| $ B_{^{69}Ga} $ | $(3.02 \pm 0.05) \times 10^{-4} \text{ cm}^{-1}$ |
| $ B_{^{71}Ga} $ | $(3.77 \pm 0.05) \times 10^{-4} \text{ cm}^{-1}$ |

This is in contrast to the description of the Mn-In pair.³

The energy levels of a $S = \frac{5}{2}$ system in a cubic crystal field with a trigonal distortion have been calculated as a function of the magnetic field. In Fig. 3 this is shown for the magnetic field oriented (a) parallel with ($\theta = 0^\circ$) and (b) perpendicular to ($\theta = 90^\circ$) the trigonal C_3 axis. In the parallel case there is no mixing of states (neglecting a small contribution from the cubic fine-structure term in the spin Hamiltonian); i.e., only $\Delta M = \pm 1$, $\Delta m = 0$ transitions are allowed. (These transitions are, however, only a part of the spectrum observed in the $\langle 111 \rangle$ direction. The other ones originate in the defects oriented along the other three trigonal directions which coincide with

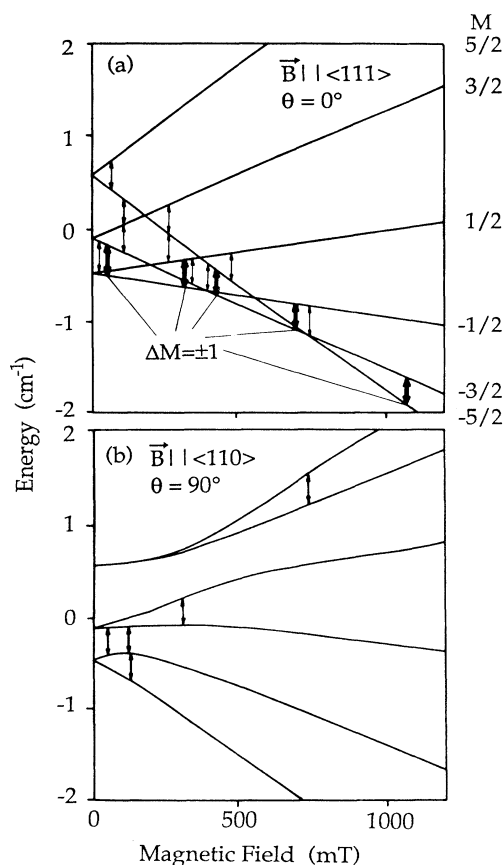


FIG. 3. Energy-level diagrams for the $(Mn_i^{2+}-Ga_s^{-})$ defect for the pair oriented (a) parallel with the magnetic field ($\mathbf{B} \parallel \langle 111 \rangle$, $\theta = 0^\circ$) and (b) perpendicular to the magnetic field ($\theta = 90^\circ$) and which occurs at $\mathbf{B} \parallel \langle 110 \rangle$ and $\mathbf{B} \parallel \langle 112 \rangle$. EPR transitions at 9.01 GHz are indicated. For an exact parallel orientation (a) only allowed, $\Delta M = \pm 1$, electronic spin transitions have a transition probability not equal to zero (bold arrows).

$\theta=70.5^\circ$ to the magnetic field.) In Fig. 3(a) the allowed transitions are marked with bold arrows and the forbidden ones with thin arrows. The intensity of the forbidden transitions are, of course, equal to zero when the magnetic field is oriented exactly along the C_3 axis of the defect, but already a small misalignment leads to measurable intensities of those transitions as well as of forbidden nuclear-spin transitions. For arbitrary directions nearly all such electronic spin transitions can be measured, as can be seen in Fig. 2.

A further proof of the correct assignment of quantum numbers to the observed EPR lines can be obtained from the positions of the forbidden hyperfine transitions observed in the high-field, fine-structure line at $\vec{B}||\langle 111 \rangle + 2^\circ$ ($\theta=2^\circ$) shown in Fig. 4. On each side of the six allowed Mn hyperfine lines ($\Delta m=0$), there are two extra lines (each split into a quartet by the Ga hyperfine interaction) which are a part of the forbidden nuclear-spin transitions (see the spectrum and the corresponding stick spectrum in Fig. 4). The positions of these forbidden ($\Delta m=\pm 1$) Mn hyperfine transitions can only be understood for electronic spin transitions $M = \pm \frac{5}{2} \leftrightarrow M' = \pm \frac{3}{2}$, since the theory predicts that only in those cases can four of the ten forbidden ($\Delta m = \pm 1$) manganese nuclear-spin transitions fall outside the six allowed ones. Because D is positive (see below), the transition shown in Fig. 4 can be identified as $M = -\frac{5}{2} \leftrightarrow M' = -\frac{3}{2}$.

The sign of the zero-field-splitting parameter D determines the sequence of the energy levels at zero magnetic field. From the analysis of the line positions as described above, it is possible to determine only the absolute value of D . The sign can, however, be determined from a comparison of the EPR intensities with the theoretical transi-

tion probabilities, including the effect of Boltzmann population for different temperatures. This was described in detail for the $(\text{Mn-In})^+$ pair.³ In the case of $(\text{Mn-Ga})^+$, we studied two lines at 720 and 310 mT in the perpendicular orientation as a function of temperature, and the result shows that the sign of D is positive. The energy-level diagrams shown in Fig. 3 are, therefore, drawn with $D = +0.1773 \text{ cm}^{-1}$.

The involvement of one Ga atom in the defect was suggested from the well-resolved $I = \frac{3}{2}$ hyperfine structure (see Fig. 1). In the following we will discuss this identification in more detail. In Fig. 5 the measured hyperfine interaction for the high-field, fine-structure line is shown with the pair oriented parallel (left) and perpendicular (right) to the magnetic field. For both of these orientations the structures are considerably simplified since only allowed Ga nuclear-spin transitions occur. It is clearly seen that the fourfold-split lines are further split, even though this splitting is not completely resolved. Gallium has two isotopes, ^{69}Ga and ^{71}Ga , with a natural abundance of 60.1% and 39.9%, respectively. Both have a nuclear spin $I = \frac{3}{2}$, but their nuclear g values differ, with $g_N^{(69)} = 1.34$ and $g_N^{(71)} = 1.71$. Using this information and the parameters given in Table I, it has been possible to successfully simulate the experimental spectra, as shown in Fig. 5. For the determination of the Ga hyperfine interaction parameter in the perpendicular case, B_{Ga} , a contribution of terms proportional to D^2/B^2 were taken into account, as was done in the case of Mn-B.²³ It should be noted that this approximation is only valid for the high-field electronic spin transition shown in Fig. 5. As expected, good agreement between experiments and simulations is obtained using the ratio between the hyperfine parameters for the two isotopes which is proportional to the ratio of their nuclear g values. This

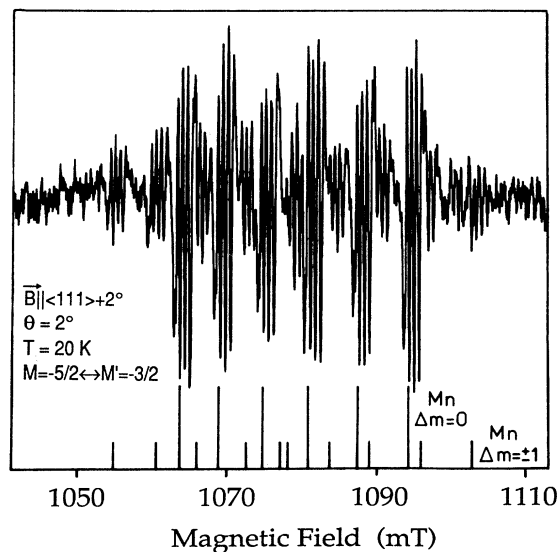


FIG. 4. Experimental hyperfine structure of the electronic spin transition $M = -\frac{5}{2} \leftrightarrow M' = -\frac{3}{2}$ for $\theta=2^\circ$ at $T=20 \text{ K}$. Allowed ($\Delta m=0$) and forbidden ($\Delta m=\pm 1$) nuclear-spin transitions of manganese are indicated in the corresponding stick spectrum by large and small sticks, respectively.

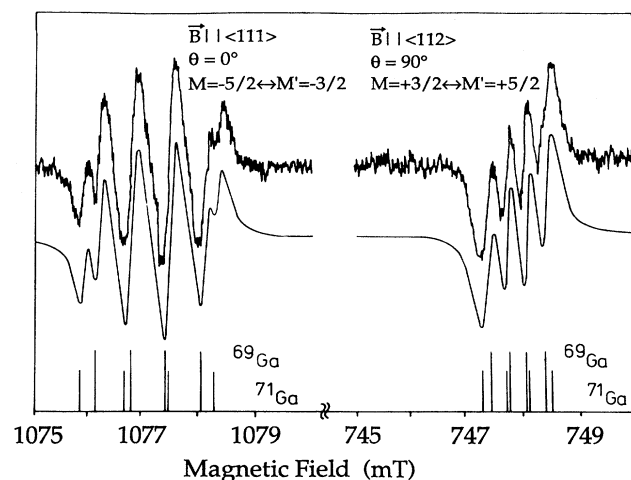


FIG. 5. Experimental (top) and calculated (bottom) Ga hyperfine structure for (left) the pair oriented parallel to the magnetic field for the $M = -\frac{5}{2} \leftrightarrow M' = -\frac{3}{2}$ electronic spin transition at $T=20 \text{ K}$ and (right) for the perpendicular orientation for the $M = \frac{3}{2} \leftrightarrow M' = \frac{5}{2}$ transition. The simulation is based on the line positions and relative isotopic intensities as shown in the stick spectra.

analysis of the gallium hyperfine interactions confirms unambiguously that one Ga atom is involved in the observed defect.

A difference in the center of gravity of the Ga hyperfine structures for the two Ga isotopes is clearly observed in the simulations of the hyperfine structure in the parallel orientation ($\theta=0^\circ$). This effect, which does not depend on the materials or preparation conditions, is largest when the magnetic field is oriented parallel to the axis of the defect. In the perpendicular direction ($\theta=90^\circ$), an optimal fit of the Ga hyperfine structure was obtained with a value of this isotope shift only half of that in the parallel direction. The isotope shift can be explained by slightly different zero-field parameters D , for the two isotopically different defects $(\text{Mn-}^{69}\text{Ga})^+$ and $(\text{Mn-}^{71}\text{Ga})^+$. In silicon isotope effects in the zero-field splitting have previously been observed in the cases of tin-vacancy²⁴ and Mn-B (Ref. 2) pairs. The difference δD between the Mn-Ga pairs containing either ^{69}Ga or ^{71}Ga is determined thus:

$$\delta D = D_{(\text{Mn-}^{71}\text{Ga})} - D_{(\text{Mn-}^{69}\text{Ga})} = -0.06 \times 10^{-4} \text{ cm}^{-1}.$$

DISCUSSION

From the experimental data on the hyperfine interactions, it was concluded that the observed EPR spectrum is caused by a pair defect consisting of one Mn and one Ga atom. Arguments have been put forward that the angular dependence of the fine structure is determined essentially by the manganese $3d^5$ center with a ${}^6S_{5/2}$ ground state in a cubic crystal field, with a strong trigonal component caused by the associated gallium. It is, therefore, suggested that the microscopic structure of the defect is a pair consisting of an interstitial Mn^{2+} ion and a substitutional Ga^- ion located in the nearest-neighbor site, i.e., a $(\text{Mn}^{2+}\text{-Ga}^-)$ pair. The atomic model and energy-level diagram of the ground state of such a defect is shown in Fig. 6. The numerous arguments in favor of this model, which have been discussed in detail for the Mn-In and Mn-B pairs,^{2,3} are also applicable to the case of the Mn-Ga pair.

As mentioned earlier, the magnitudes of the trigonal zero-field splitting and the Zeeman splitting in the magnetic-field range at which the EPR transitions occur are very similar (an intermediate case). Therefore, in the analysis of the Mn-Ga EPR spectrum, a direct diagonalization of the energy matrix of the electronic parts of the spin Hamiltonian was required. The result of this analysis was that both the positions and intensities of all

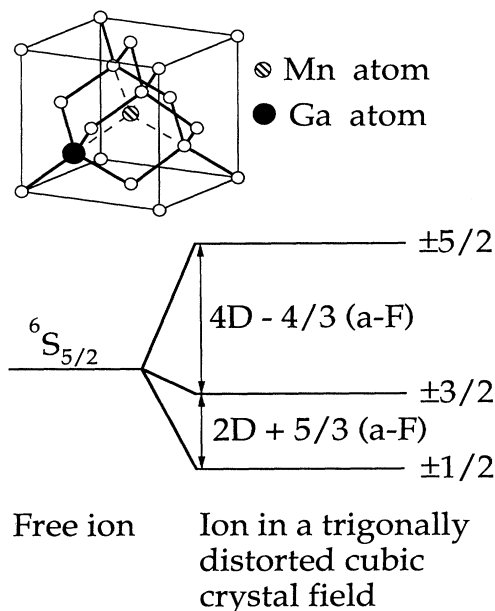


FIG. 6. Energy-level diagram of the interstitial Mn^{2+} ground state in the trigonal $(\text{Mn-Ga})^+$ defect. The inset shows the atomic model of the $(\text{Mn-Ga})^+$ pair in silicon.

lines could be explained. In particular, no traces of other spectra revealing Mn-Ga pair configurations of lower symmetry than trigonal could be observed. This is in line with the observations made on the other Mn-acceptor pairs investigated so far.³ The reasons for the difference between the Fe-acceptor pairs, where trigonal and orthorhombic centers as well as a conversion between both configurations have been observed, and the apparently stable trigonal configuration of the Mn-acceptor pairs might be, first, the different Coulomb forces between the single negative acceptor ion and the single positive Fe ion or the double positive Mn ion, respectively, and, second, different lattice relaxations for the incorporation of Fe or Mn nearby the acceptor.

The physical behavior and microscopic models for the known Mn-acceptor pairs are almost identical. They differ mainly in the strength of the trigonal crystal field caused by the various group-III acceptor ions. In the EPR experiments this is reflected in the D parameter (Table II). Since almost all Mn-group-III acceptor pairs have been investigated, it is interesting to compare the magnitudes of D for the different acceptors. In Table II we have included $R[A(3+)] - R[\text{Si}(4+)]$, the difference in ionic radii between the replacing acceptors and silicon.

TABLE II. Trigonal zero-field-splitting parameters D , isotope effect in D , δD , and the difference in the ionic radii (from Ref. 25) between the acceptor A and Si, $\Delta R = R[A(3+)] - R[\text{Si}(4+)]$, for the Mn^{2+} -group-III acceptor pairs in silicon.

| | | D (cm^{-1}) | δD (cm^{-1}) | ΔR (\AA) |
|--------------------|------------|--------------------------|--|-----------------------------|
| $(\text{Mn-B})^+$ | Ref. 2 | 0.0511 | $D(\text{Mn-}^{11}\text{B}) - D(\text{Mn-}^{10}\text{B}) = -1 \times 10^{-4}$ | -0.18 |
| $(\text{Mn-Al})^+$ | Ref. 1 | 0.0185 | | +0.11 |
| $(\text{Mn-Ga})^+$ | this paper | 0.1773 | $D(\text{Mn-}^{71}\text{Ga}) - D(\text{Mn-}^{69}\text{Ga}) = -0.06 \times 10^{-4}$ | +0.19 |
| $(\text{Mn-In})^+$ | Ref. 3 | 0.52 | | +0.38 |

The ionic radii were based on the simplified assumption that a Si crystal consists of residual Si ions in the 4+ oxidation state and paired binding electrons. In this picture the occupied acceptor has an oxidation state of 3+. The ionic radii of Si(4+) and A(3+), with A = B, Al, Ga, and In, were taken from Ref. 25.²⁶ A plot of D as a function of $R[A(3+)] - R[Si(4+)]$ is shown in Fig. 7. It is interesting to note that regardless of whether the Mn-acceptor pair contains acceptors which are larger (Al, Ga, In) or smaller (B) than silicon, it leads to the same sign of the D value. Furthermore, as was already guessed in Ref. 3, in the case of Mn-group-III acceptor pairs, it seems that the bigger the size difference between the acceptor and silicon atom, the larger the zero-field parameter D .

On the other hand, a dependence of D on the different isotopes of the acceptors was observed for the Mn-Ga and Mn-B pairs. This isotope effect is, however, more than 3 orders of magnitude smaller than the differences in D values discussed above. Therefore, we conclude that the reasons for the different D values for different acceptors and the isotope effect on D are not the same. It has been argued that the origin of the isotope shift in the fine structure is essentially vibronic.^{24,27-29} In this model the vibrations of the atoms which influence the resulting electric field are slightly different for different isotope masses, and as a result, the zero-field parameter D differs for different isotopes. The relative isotope shift of the zero-field splitting parameters, $\delta D/D$, is in this model proportional to the relative mass change $\delta M/M$. The measured relative isotopic effect for Mn-Ga is $|\delta D/D| = 1.75 \times 10^{-5}$ per unit mass change and, for Mn-B, $|\delta D/D| = 2 \times 10^{-3}$ per unit mass change (boron has the two isotopes ¹⁰B and ¹¹B),² while in the case of Mn-In, no isotope effect could be resolved (since In has two isotopes with ¹¹³In and ¹¹⁵In, with a natural abundance of 96% and 4%, respectively).³ This is in agreement with the fact that the relative mass change $\delta M/M$ is much larger for light elements than for heavier ones.

CONCLUSIONS

An observation of a manganese-gallium pair in silicon is reported. From an EPR investigation, the chemical identity is proved from hyperfine interactions with both

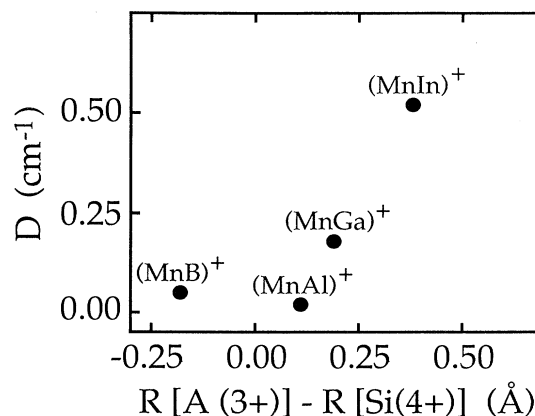


FIG. 7. Dependence of the trigonal zero-field parameter D of the Mn^{2+} -group-III acceptor pairs as a function of the difference between the ionic radii of silicon Si(4+) and the replacing acceptor A(3+).

manganese and gallium. The defect shows trigonal symmetry and an unusually complicated fine-structure behavior because the trigonal zero-field splitting and the Zeeman splitting in the experiments are very similar. As a result of a direct diagonalization of the energy matrix, it is shown that the experimental data can be successfully explained assuming a ${}^6S_{5/2}$ ground state of a Mn^{2+} ion which is split by a strongly trigonally distorted cubic crystal field caused by a nearest-neighbor Ga^- ion. Isotope effects in the fine-structure parameter D are also measured, and from a comparison between different Mn-acceptor pairs, it is suggested that the magnitude of D depends mainly on the size of the acceptors.

ACKNOWLEDGMENTS

The authors would like to thank Dr. A. A. Lebedev (Physico-Technical Institute, Leningrad) for supplying highly gallium-doped samples, U. Rehse for his support in the computer calculations, and I. Gründler for technical assistance. We would also like to thank G. Watkins for useful comments on the manuscript. The work was supported by grants from the Swedish Natural Science Research Council and the Swedish National Board for Technical Development.

¹G. W. Ludwig and H. H. Woodbury, in *Solid State Physics*, edited by F. Seitz and D. Turnbull (Academic, New York, 1962), Vol. 13, p. 223.
²J. Kreissl and W. Gehlhoff, *Phys. Status Solidi B* **112**, 695 (1982).
³J. Kreissl, W. Gehlhoff, P. Omling, and P. Emanuelsson, *Phys. Rev. B* **42**, 1731 (1990).
⁴H. Dietrich, H. Vollmer, and R. Labusch, *Solid State Commun.* **58**, 811 (1986).
⁵J. Kreissl and W. Gehlhoff, *Phys. Status Solidi B* **145**, 609 (1988).
⁶H. Lemke, *Phys. Status Solidi A* **64**, 549 (1981); **76**, 223 (1983).
⁷K. P. Abdurakhmanov, A. A. Lebedev, J. Kreissl, and Sh.B. Utamuradova, *Fiz. Tekh. Poluprovodn.* **19**, 213 (1985) [Sov.

Phys. Semicond. **19**, 133 (1985)].
⁸M. Heider, H. Sitter, R. Czaputa, H. Feichtinger, and J. Oswald, *J. Appl. Phys.* **62**, 3785 (1987).
⁹H. Conzelmann, *Appl. Phys. A* **42**, 1 (1987).
¹⁰T. Bever, P. Emanuelsson, M. Kleverman, and H. G. Grimmeiss, *Appl. Phys. Lett.* **55**, 2541 (1989).
¹¹A. Zunger, in *Solid State Physics*, edited by H. Ehrenreich, F. Seitz, and D. Turnbull (Academic, New York, 1986), Vol. 39, p. 275.
¹²F. Beeler, O. K. Andersen, and M. Scheffler, *Phys. Rev. B* **41**, 1603 (1990).
¹³J. J. van Kooten, G. A. Weller, and C. A. J. Ammerlaan, *Phys. Rev. B* **30**, 4564 (1984).
¹⁴W. Gehlhoff, K. Irmscher, and U. Rehse, in *Defects in Semi-*

- conductors, Vol. 38-41 of *Materials Science Forum*, edited by G. Ferenczi (Trans Tech, Aedermannsdorf, Switzerland, 1989), p. 373.
- ¹⁵P. Omling, P. Emanuelsson, W. Gehlhoff, and H. G. Grimmeiss, *Solid State Commun.* **70**, 807 (1989).
- ¹⁶W. Gehlhoff, P. Emanuelsson, P. Omling, and H. G. Grimmeiss, *Phys. Rev. B* **41**, 8560 (1990).
- ¹⁷A. Chantre and D. Bois, *Phys. Rev. B* **31**, 7979 (1985).
- ¹⁸A. Chantre and L. C. Kimerling, in *Defects in Semiconductors*, Vol. 10-12 of *Materials Science Forum*, edited by H. J. von Bardeleben (Trans Tech, Aedermannsdorf, Switzerland, 1986), p. 373.
- ¹⁹K. Irmscher and J. Kreissl, *Phys. Status Solidi A* **116**, 755 (1989).
- ²⁰H. Feichtinger, J. Oswald, R. Czaputa, P. Vogel, and K. Wüstel, in *Proceedings of the Thirteenth International Conference on Defects in Semiconductors*, edited by L. C. Kimerling and J. M. Parsey, Jr. (The Metallurgical Society of AIME, New York, 1984), Vol. 14a, p. 855.
- ²¹See Refs. 2 and 3. Note that in Refs. 2 and 3 the crystal-field terms [Eq. (3) in this paper] are incorrect due to misprints. However, in the calculations in these papers, the correct formula (given here) has been used.
- ²²M. T. Hutchings, in *Solid State Physics*, edited by F. Seitz and D. Turnbull (Academic, New York, 1964), Vol. 16, p. 227.
- ²³Note that, because of misprint, the term $D^2/(8H^2)$ in Eq. (3), Ref. 2, is written as $D^2/(8M^2)$.
- ²⁴G. D. Watkins, *Solid State Commun.* **17**, 1205 (1975).
- ²⁵*Atom und Molekularphysik, Teil 4: Kristalle*, edited by K. H. Hellwege, Landolt-Börnstein, Vol. I (Springer-Verlag, Berlin, 1955), p. 523.
- ²⁶It should be noted that there is a scatter in the values of the ionic radii in the literature; see, e.g., S. Fraga, J. Karwowski, and K. M. S. Saxena, *Handbook of Atomic Data* (Elsevier, Amsterdam, 1976).
- ²⁷S. A. Marshall, J. A. Hodges, and R. A. Serway, *Phys. Rev.* **136**, A1024 (1964).
- ²⁸S. A. Marshall, *Phys. Rev.* **159**, 191 (1967).
- ²⁹K. M. Lee, Le Si Dang, and G. D. Watkins, *Phys. Rev. B* **32**, 2273 (1985).